ISBN: 978-3-95450-201-1 doi:10.18429/JACoW-IBIC2018-WEPC04

SETUP FOR BEAM PROFILE MEASUREMENTS USING OPTICAL TRANSITION RADIATION*

J. Pforr†, M. Arnold, T. Bahlo, L. Jürgensen, N. Pietralla, A. Rost,
TU Darmstadt, Darmstadt, Germany
F. Hug, Johannes Gutenberg-Universität Mainz, Mainz, Germany

Abstract

The S-DALINAC is a thrice-recirculating, superconducting linear electron accelerator at TU Darmstadt. It can provide beams of electrons with energies of up to 130 MeV and currents of up to 20 µA. The accelerator performance was improved by an extension of the beam diagnostics, as this increases the reproducibility of the machine settings. In addition, the installation of several beam profile measurement stations is planned, which should be operational down to a beam current of 100 nA, as this current is used for beam tuning. Combining these devices with a quadrupole scan also allows for emittance measurements. The beam profile measurements shall be done based on optical transition radiation (OTR), resulting from the penetration of relativistic electrons from vacuum into a metal target. The radiation can be detected using standard cameras that provide information on the two-dimensional particle distribution. This contribution will address the layout of the measurement stations and a first test measurement will be presented.

NEW DIAGNOSTIC STATIONS AT THE S-DALINAC

The current layout of the S-DALINAC is shown in Fig. 1. The electron beam coming from one of the two sources can be accelerated in the superconducting injector to up to 10 MeV beam energy [1]. After the injector the beam can be used at the DHIPS (Darmstadt High Intensity Photon Setup) experimental area [2] or be bent into the main linac. The electrons can pass the main linac up to four times due to the three existing recirculations [3] and are afterwards extracted to the experimental hall with a maximum energy of 130 MeV.

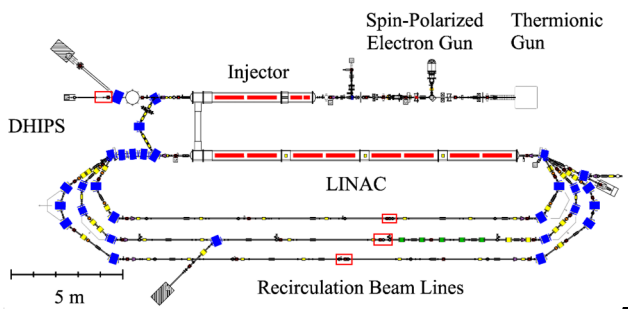

Figure 1: Layout of the S-DALINAC with three recirculation beam lines. The red boxes denote the positions of the planned diagnostic stations.

In order to enable an emittance measurement after each acceleration, there are several diagnostic stations necessary. One is located behind the superconducting injector and further diagnostic stations are planned in the straight sections of each recirculation beam line. The positions were chosen such that quadrupoles are available for an emittance measurement based on a quadrupole scan. In addition, the diagnostic stations consist of an OTR target and CMOS cameras (FLIR BFLY-PGE-31S4M-C) which detect the radiation. This type of camera was chosen for various reasons as a high resolution and framerate. Of special importance is the possibility to adjust many camera parameters, e.g. the exposure time and gain, remotely, which results in a high flexibility. As these cameras have to be protected from radiation damage, the target is supposed to be observed via a mirror in order to allow for better shielding.

OPTICAL TRANSITION RADIATION

Transition radiation is emitted when a relativistic charged particle crosses the boundary between two media with different permittivity, as the electric field has to rearrange at the boundary. This radiation was predicted in 1947 by Ginzburg and Frank [4], and after pioneering work by Wartski [5] it has been established as a tool for electron beam diagnostics. The emission of OTR is directed in two cones with opening angle of $1/\gamma$, as depicted in Fig. 2, where the metal target is inclined with 45° with respect to the electron beam. The radiated power for an electron with Lorentz factor $\gamma >> 1$ can be described by [6]

$$W_1(\theta) = \frac{e^2}{4\pi^3\epsilon_0 c}\frac{\beta^2\sin^2\theta}{(1-\beta^2\cos^2\theta)^2}$$

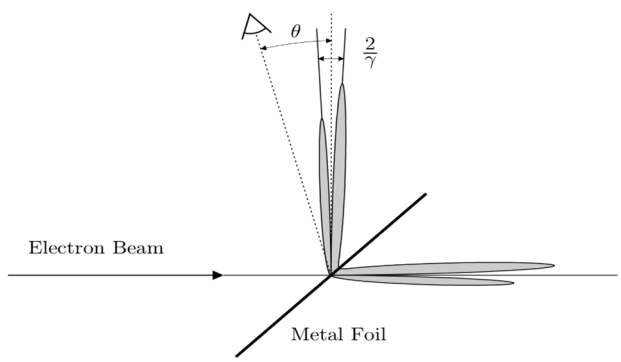

Figure 2: The directional dependence of the intensity of OTR light that is emitted by a metal foil with 45° angle to the electron beam [7].

* Work supported by DFG through GRK 2128.
† jpforr@ikp.tu-darmstadt.de

Content from this work may be used under the terms of the CC BY 3.0 licence (© 2018). Any distribution of this work must maintain attribution to the author(s), title of the work, publisher, and DOI.

ISBN: 978-3-95450-201-1 doi:10.18429/JACoW-IBIC2018-WEPC04

where $W_1 = d^2W/d\omega d\Omega$ is the spectral distribution of the energy and $\beta = v/c$ the particle velocity. Additionally, for further considerations concerning the most suited target materials, it shall be noted that the total intensity of the radiation is proportional to both γ and the plasma frequency, which is the natural frequency of electron oscillation in a metal, of the target material [8].

TARGET DESIGN

For the target design, different aspects have to be taken into account. As the OTR intensity is proportional to the target plasma frequency, this is an important parameter for the choice of the target material. The plasma frequencies of some metals are summarized in Table 1.

Table 1: Plasma Frequencies of Common Materials [9].

Material	Plasma Frequency [eV]
Aluminium	15
Nickel	9.45
Gold	5.8
Silver	3.735

Due to the high plasma frequency of aluminium, this material is favoured for the OTR targets. Another issue, however, is the target flatness. Due to the directed nature of OTR, any surface modulation will also translate into an intensity modulation in the image. Therefore, not only pure aluminium targets are considered, but also targets which consist of a µm-thin aluminium layer deposited on a kapton (polyimide) foil. As the kapton can be stretched, a flat surface is easier to achieve. In order to realise the stretching of the target foil, a target holder was designed that keeps the target under tension. The resulting diameter of the target foil is 25 mm, the thickness is mainly determined by thermal properties. The temperature change of the target foil is described semi-empirically by [10]

$$\frac{\Delta T(r,t)}{\Delta t} = \frac{1}{c_p \rho}\left[\frac{dE}{dx}\rho \exp\left(-\frac{r^2}{2\sigma^2}\right) N(t) - k\nabla^2 T(r,t) - \frac{2\epsilon\sigma_s}{\delta}\left(T(r,t)^4 - T_0^4\right)\right]$$

where dE/dx denotes the stopping power, N(t) the (possibly time-dependent) particle flux, k the thermal conductivity, ε the emissivity and δ the target thickness. It shall be noted that in this equation the assumption of a spatial gaussian distribution of the beam was made. The obvious consequence for the target design is that thin targets are advantageous for thermal aspects. For further considerations, the properties of aluminium and kapton are summarized in Tab. 2. From these quantities we can conclude that aluminium can conduct heat better, but emits less energy than kapton by thermal radiation. In order to investigate the relevance of these effects, a simulation of the thermal behaviour of the target was conducted.

Table 2: Thermal Properties of Aluminium and Kapton

	Aluminium	Kapton
Density [g/cm³]	2.7	1.4
Thermal conductivity [W/(Km)]	250	0.2
Emissivity	0.04	0.24

THERMAL SIMULATIONS

This simulation of the thermal target properties is supposed to give a rough estimate of the heating of both, an aluminium and a kapton target. It was conducted with CST MPhysics Studio [11]. At first, the total deposited power had to be estimated for an expected target thickness of 10 µm. Considering the stopping power only the energy deposition by collisions is relevant [12], which has only a slight energy-dependence, so typical values of the stopping power were used. The resulting power for the maximum beam current of 20 µA results to 0.06 W for kapton and 0.10 W for aluminium. While these values seem small, a uniformly distributed beam spot with a radius of 0.5 mm results in a heated volume of only 8e-3 mm³, so a significant heating has to be expected. In the model, the target foil was surrounded by an aluminium target holder, which is similar to a heat reservoir due to the thickness of 4 mm. The outer boundaries of this target holder were isothermal. The results for a pure aluminium target and a kapton target are

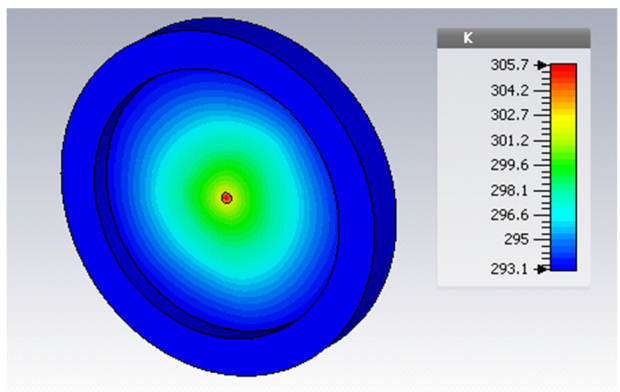

Figure 3: The temperature distribution of an aluminium target for 20 µA. Simulated with CST [11].

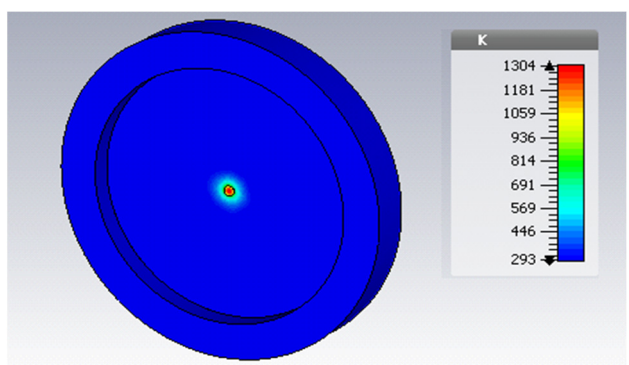

Figure 4: The temperature distribution of a kapton target for 20 µA. Simulated with CST [11].

Content from this work may be used under the terms of the CC BY 3.0 licence (© 2018). Any distribution of this work must maintain attribution to the author(s), title of the work, publisher, and DOI.

ISBN: 978-3-95450-201-1 doi:10.18429/JACoW-IBIC2018-WEPC04

Content from this work may be used under the terms of the CC BY 3.0 licence (© 2018). Any distribution of this work must maintain attribution to the author(s), title of the work, publisher, and DOI.

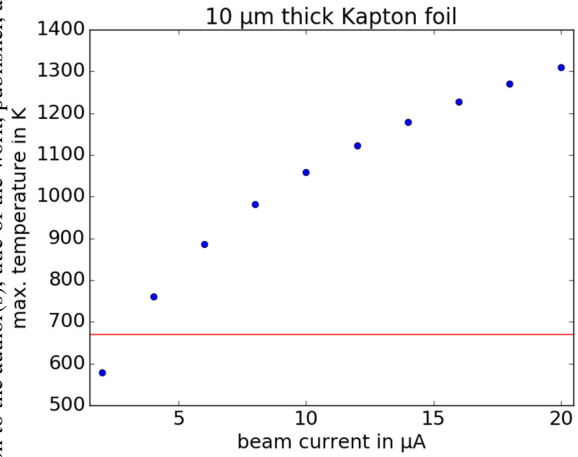

Figure 5: The maximum temperature of a kapton target for various beam currents. The red line denotes 400°C, which we consider the maximum reasonable temperature. This is no strict limit, however, thermal aging takes place and destroying the target must be avoided. Simulated with CST [11].

shown in Fig. 3 and Fig. 4 respectively. It is noticeable that the heat is distributed over a large volume in aluminium due to the high thermal conductivity, while there is only a small heated spot on the kapton target. Consequently, the aluminium target is hardly warmed up, while the kapton target reaches a temperature of 1300 K, which would destroy the kapton. For that reason, for the kapton target a beam current limit has to be found. Therefore, the dependency of the maximum temperature from the beam current was investigated. The results are summarized in Fig. 5. The calculations show that only beam currents of a few µA are possible without destroying the kapton target. For smaller beamspots this limit would be reduced even further, so a safety margin is necessary as long as the actual beam spot size is unknown. However, the demonstration measurements described in the next section show that a beam size measurement can be conducted at low beam current and energy with sufficient image brightness.

DEMONSTRATION MEASUREMENT

To demonstrate the applicability of this technique, in Dec. '17 a first emittance measurement with an OTR target was conducted [13]. The target is located behind the superconducting injector, where the beam energy was 5.2 MeV in this beamtime. We used beam currents of ~100 nA, as the target image was sufficiently bright, but not saturated. Fig. 6 shows one example image. Despite the fact that the beamspot does not have a 2D-gaussian shape, the horizontal and vertical projections allowed an easy evaluation. After a background substraction and a calibration of the image size, the beam size could be determined by a gaussian fit. This allowed to determine the emittances, which are on the order of 0.1 mm mrad with typical uncertainties of less than 10 % [13].

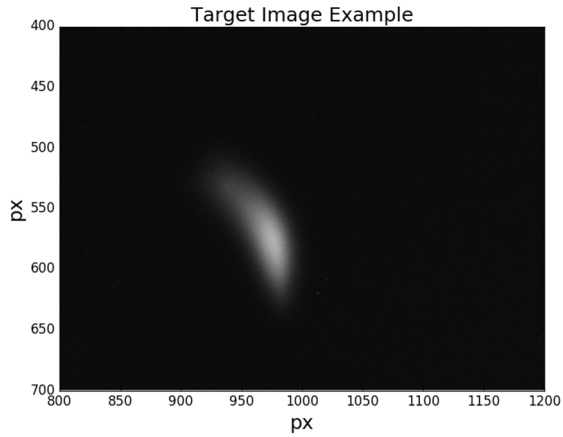

Figure 6: Section of an OTR target image example.

CONCLUSION AND OUTLOOK

The design considerations of OTR targets for an emittance measurement setup at the S-DALINAC show different options. One option would be to construct targets based on a Kapton foil with a small layer of aluminium added. In this case, the targets can not stand the full beam current of 20 µA but can be used for low current operation (e.g. during beam tuning). On the other hand, pure aluminium targets can withstand the maximum beam current, however, their flatness is problematic. Therefore, the production of kapton-based targets has started. Apart from that, the design of the optics setup and shielding for the camera is ongoing work. Currently, it is planned to conduct an emittance measurement later this year.

REFERENCES

[1] Norbert Pietralla, "The Institute of Nuclear Physics at the TU Darmstadt", *Nuclear Physics News*, vol. 28, no. 2, pp. 4-11, 2018, DOI: 10.1080/10619127.2018.1463013

[2] K. Sonnabend *et al.*, "The Darmstadt High-Intensity Photon Setup (DHIPS) at the S-DALINAC", *Nucl. Instr. Meth.*, vol. 640, pp. 6-12, 2011.

[3] M. Arnold *et al.*, "Construction and Status of the Thrice Recirculating S-DALINAC", in *Proc. 8th Int. Particle Accelerator Conf. (IPAC'18)*, Copenhagen, Denmark, May 2017, paper TUPAB030, pp. 1384-1387, https://doi.org/10.18429/JACoW-IPAC2017-TUPAB030

[4] V. L. Ginzburg and I. M. Frank, "Radiation of a uniformly moving electron crossing a boundary between two media", JETP 16, p. 15, 1946.

[5] L. Wartski, S. Roland, J. Lasalle, M. Bolore, G. Filippi, *Jour. Appl. Phys.,* Vol. 46, 1975, 3644, doi: 10.1063/1.322092

[6] V. L. Ginzburg and V. N. Tsytovich, "Several problems of the theory of transition radiation and transition scattering", *Phys. Rep*. 49, pp. 1-89, 1979.

[7] H. Loos, "Bestimmung der longitudinalen Struktur der Elektronenbunche im Strahl von supraleitenden Beschleunigern", Ph.D. thesis, Phys. Dept., TU Darmstadt, Darmstadt, Germany, 2001.

ISBN: 978-3-95450-201-1 doi:10.18429/JACoW-IBIC2018-WEPC04

[8] S. Döbert *et al.*, "Beam Diagnostics using Transition Radiation", in *Proc. Workshop on RF Superconductivity*, Gif-sur-Yvette, France, Oct. 1995, pp. 719-722.

[9] D. Langley, R. A. Coutu Jr., L. A. Starman, and S. Rogers, "Optical Metamaterials for Photonics Applications", *Proc. SPIE – The International Society of Optical Engineering*, vol. 7468, 2009.

[10] E. Bravin, T. Lefèvre and C. Vermare, "OTR Studies for the High Charge CTF3 Beam", *Proc. Particle Accelerator Conference (PAC),* Portland, Oregon, USA, May 2003, pp. 2464-2466.

[11] Dassault Systèmes: CST – Computer Simulation Technology GmbH: CST Studio Suite. Version 2016, http://www.cst.com/.

[12] E. Bravin, "Thermal analysis of OTR screens for CTF3", CTF3 Note 019, 2001.

[13] F. Hug, M. Arnold, T. Bahlo, J. Pforr, and N. Pietralla, "Beam Based Alignment of SRF Cavities in an Electron Injector Linac", *Proc. 9th Int. Particle Accelerator Conf. (IPAC '18),* Vancouver, Canada, May 2018, paper THPMF064, pp. 4219-4222.

Content from this work may be used under the terms of the CC BY 3.0 licence (© 2018). Any distribution of this work must maintain attribution to the author(s), title of the work, publisher, and DOI.